



HAL
open science

Evidence for molecular structural variations in the cytoarchitectures of a Jurassic plant

Yuangao Qu, Nicola Mcloughlin, Mark van Zuilen, Martin Whitehouse, Anders Engdahl, Vivi Vajda

► **To cite this version:**

Yuangao Qu, Nicola Mcloughlin, Mark van Zuilen, Martin Whitehouse, Anders Engdahl, et al.. Evidence for molecular structural variations in the cytoarchitectures of a Jurassic plant. Geological Society of America | GEOLOGY, 2019, 47, 10.1130/G45725.1 . insu-02400891

HAL Id: insu-02400891

<https://insu.hal.science/insu-02400891>

Submitted on 9 Dec 2019

HAL is a multi-disciplinary open access archive for the deposit and dissemination of scientific research documents, whether they are published or not. The documents may come from teaching and research institutions in France or abroad, or from public or private research centers.

L'archive ouverte pluridisciplinaire **HAL**, est destinée au dépôt et à la diffusion de documents scientifiques de niveau recherche, publiés ou non, émanant des établissements d'enseignement et de recherche français ou étrangers, des laboratoires publics ou privés.

Evidence for molecular structural variations in the cytoarchitectures of a Jurassic plant

Yuangao Qu^{1,2*}, Nicola McLoughlin^{3,4}, Mark. A. van Zuilen⁵, Martin Whitehouse², Anders Engdahl⁶, and Vivi Vajda^{2*}

¹Institute of Deep-Sea Science and Engineering, Chinese Academy of Sciences, Sanya 572000, China

²Swedish Museum of Natural History, 114 18 Stockholm, Sweden

³Department of Geology, Rhodes University, Grahamstown 6139, South Africa

⁴Albany Museum, Grahamstown 6139, South Africa

⁵Equipe Géomicrobiologie, Institut de Physique du Globe de Paris, Sorbonne Paris Cité, UMR 7154 CNRS, Université Paris Diderot, 75013 Paris, France

⁶MAX IV Laboratory, Lund University, SE-221 00 Lund, Sweden

ABSTRACT

In this study, we investigate the molecular structural characteristics of organic remains in various cellular organelles from a 180 Ma Jurassic royal fern belonging to the Osmundaceae family of ferns, and compare their carbon isotopic compositions to a now-living species of royal fern (*Osmunda regalis*). We discovered molecular structural variations indicated by Raman and infrared spectral parameters obtained from various fossilized cellular organelles. The organic remains preserved in the chromosomes and cell nuclei show marked structural heterogeneities compared to the cell walls during different stages of the cell cycle. The fossil and extant fern have similar $\delta^{13}\text{C}$ values obtained from bulk samples, supporting evolutionary stasis in this plant lineage and an unchanged metabolic pathway of carbon assimilation since the Jurassic. The organic remains in the cellular organelles of the fossil seem to be less heterogeneous than those in the extant fern, likely due to the preferential preservation of certain cellular compounds during fossilization. Taphonomic processes appear to have diminished the subcellular isotopic heterogeneities. Our research sheds light on the functioning of ancient plant cellular organelles during mitosis, provides insights to the taphonomic processes operating at molecular and isotopic levels, and shows the practicability of *in situ* techniques in studying the evolution and behaviors of ancient cells.

INTRODUCTION

Exceptional preservation of fossilized cellular organelles is extremely rare but highly significant as these structures provide details of the evolution of life and functioning of ancient cells. The oldest fossilized cells with preserved ultrastructures can be traced to the putative planktonic organisms preserved in the 3.2 Ga Moodies Group, South Africa (Javaux et al., 2010). Complex intracellular organelles such as pyrenoids, nuclei, and lipid vesicles have been reported from Neoproterozoic strata (e.g., Hagadorn et al., 2006). Some of them, however, are still controversial and argued to be encysting protists (Huldtgren et al., 2011) or mineral inclusions such as apatite (Schiffbauer et al., 2012). More-abundant and highly diverse cells containing clear subcellular structures have

been found within fossilized Phanerozoic land plants (e.g., Remy et al., 1994). In particular, a petrified Jurassic fern belonging to the family of royal ferns (Osmundaceae) from the Korsaröd locality, southern Sweden, contains exceptionally preserved cytoarchitectures, including cytoplasm, cytosol granules, nuclei, and chromosomes (Bomfleur et al., 2014).

Previous studies on the preservation of fossilized cells largely report morphological observations using imaging techniques such as scanning electron microscopy (e.g., Bomfleur et al., 2014), transmission electron microscopy (e.g., Hagadorn et al., 2006; Javaux et al., 2010), and X-ray transmission microscopy (Huldtgren et al., 2011; Schiffbauer et al., 2012), but fewer studies use a combination of Raman spectroscopy, Fourier-transform infrared spectroscopy (FTIR), and secondary-ion mass spectrometry (SIMS) to

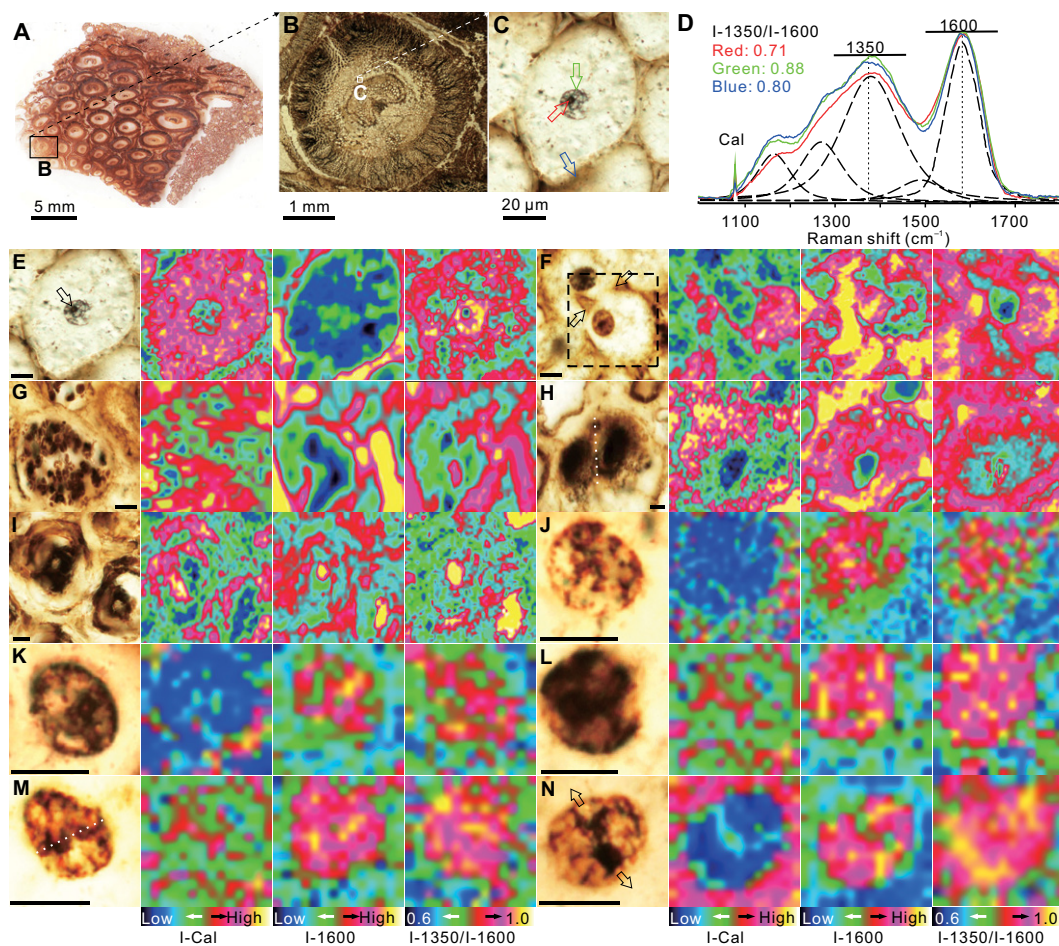
investigate the molecular structural and isotopic characteristics of organic remains preserved in fossils (Qu et al., 2018). Here we take the petrified royal fern fossil from the Korsaröd site in southern Sweden as an example, and further expand the investigation of molecular structural and isotopic characteristics of organic remains in various cytoarchitectures. We aim to explore the behaviors of organelles during the cell cycle of ancient fern, and test the use of *in situ* techniques for investigating the molecular structural and isotopic characteristics of organic remains in various fossilized cytoarchitectures. We further aim to better understand the taphonomic processes and their effects on the preservation of organic carbon, and in particular cellular components in volcanic “Konservat-Lagerstätten” deposits.

METHODS

One fossil specimen (Osmundaceae) was provided by the Swedish Museum of Natural History, Stockholm. The comparative extant fern *Osmunda regalis* was obtained from the Botanical Garden in Lund, Sweden. Two polished thin sections (~40 μm thick) from the fossil were prepared for petrographic and Raman analyses at the University of Bergen, Norway, and the PARI analytical platform at the Institut de Physique du Globe de Paris. The FTIR analyses were performed on two doubly polished wafers of the fossil at Beamline D7 in the MAX III ring in Lund, Sweden. The same Raman spectroscopic and FTIR analyses were performed on the extant royal fern, but unfortunately the signal bands cannot be distinguished from the high background noise and/or baseline and absorption. The SIMS analysis was performed on the gold-coated

*E-mails: quyg@idsse.ac.cn; vivi.vajda@nrm.se

Figure 1. A–C: Optical microscope images of a cell in sclerenchyma ring of a fossil royal fern (*Osmundaceae*). Colored arrows in C show analyzed positions with spectra in corresponding colors in D. **D:** Example Raman spectra obtained from cell in sclerenchyma ring. I-1350/I-1600 is the intensity ratio of the 1350 cm^{-1} band versus the 1600 cm^{-1} band. Dashed curves represent the decomposition of bands at 1350 cm^{-1} and 1600 cm^{-1} into a series of sub-bands. **E–N:** Raman maps of parameters I-Cal (intensity of 1086 cm^{-1} band), I-1600, and I-1350/I-1600, indicating abundances of calcite, carbonaceous material, and its molecular structural order, respectively. Corresponding optical microscopic images are at the left in each panel (scale bars = 10 μm). **E:** Nucleus in interphase with clear nucleolus (arrow). **F:** Protoplasm and daughter nuclei separated into two parts by furrow (arrows) in cytokinesis. **G:** Organic remains derived from protoplasm. **H:** Cell plate formed (dotted line) in telophase. **I:** Shrunken protoplasm. **J:** In prophase, chromosomes distributed randomly within nuclear matrix. **K,L:** Condensed chromosomes in cracked nuclear envelope during prometaphase. **M:** Chromosomes gathered near equator (dotted line) during metaphase. **N:** Chromosomes and/or chromatids starting to move toward opposite sides (arrows).



surface of three polished samples (one fossil and two extant samples) at the Swedish Museum of Natural History. The carbon isotopic analysis on two bulk samples (one fossil and one extant) was carried out at the University of Bergen. More details of sampling, geological background, analytical methods, and strategies of data acquisition are presented in the GSA Data Repository¹.

RESULTS

The fossil royal fern was entirely permineralized by calcite (Figs. 1A–1C) directly following its burial by volcanic lahar deposits at ca. 180 Ma, capturing cells in various stages of the cell cycle (Figs. 1E–1N). The Raman spectra of the fossil fern (Fig. 1D) indicate the presence of disordered carbonaceous material, with two main broad bands at ~1350 cm^{-1} and 1600 cm^{-1} consisting of a group of sub-peaks (Fig. 1D) that can be assigned to various modes of bond vibration in amorphous organic molecules (Qu et al., 2015, and references therein). Here we describe

the spectra using the intensity ratio I-1350/I-1600, reflecting the molecular structural order of carbonaceous material (Qu et al., 2015). Some spectra contain an additional sharp peak at 1086 cm^{-1} (Fig. 1D), representing the calcite mineral matrix. Raman mapping performed on the fossil fern shows that the relative abundance of calcite (indicated by the intensity of the 1086 cm^{-1} band [I-Cal]) is complementary to that of organic matter (indicated by the intensity of the 1600 cm^{-1} band [I-1600]) (Figs. 1E–1N). The I-1350/I-1600 values, indicating molecular structural order of the organic matter, vary markedly and span larger ranges in the nuclei and cytoplasm than in the cell walls (Figs. 1C–1N and 2). Their variations seem to correspond to the morphology of various cytoarchitectures during different stages of the cell cycle (Figs. 1C–1N).

The FTIR spectra obtained from the fossil have distinct absorbance bands at 2850 cm^{-1} , 2925 cm^{-1} , and 2955 cm^{-1} (Fig. 3A), corresponding to the stretching vibrations of symmetric CH_2 and asymmetric CH_2 and CH_3 , respectively. The intensities of the bands at 2925 cm^{-1} and 2955 cm^{-1} show the relative abundance of organic matter in the cytoarchitectures (I-2925 and I-2955 in Fig. 3). The IR parameter $R_{3/2}$, defined as the intensity ratio of the 2955 cm^{-1} versus the 2925 cm^{-1} band, is widely used to describe the

branching index of carbon chains (Igisu et al., 2009; Qu et al., 2017). The $R_{3/2}$ values obtained from the cell walls are higher than those from the cytoplasm (Fig. 2), which is further illustrated by IR maps (Fig. 3B).

Organic matter in the bulk samples of the fossil has a $\delta^{13}\text{C}_{\text{org-bulk}} = -27.7\text{‰}$ (Vienna Peedee belemnite), and in the extant specimens has a $\delta^{13}\text{C}_{\text{org-bulk}} = -29.5\text{‰}$ (Fig. 2). More-pronounced $\delta^{13}\text{C}$ variations (up to 7.0‰ in the fossil and 22.1‰ in the extant fern) occur within different cytoarchitectures as measured *in situ* by SIMS (Figs. 2, 4A, and 4B). Both the fossil and the extant fern have lower absolute values of $\delta^{13}\text{C}_{\text{org-SIMS}}$ than the respective bulk samples (Fig. 2). The counts of $^{12}\text{C}^{14}\text{N}$ ions in the ion images (Fig. 4) provide a semiquantitative representation of the intracellular abundance and spatial distribution of organic matter, which are consistent with the Raman and FTIR maps (I-1600 in Figs 1E–1N; I-2925 and I-2955 in Fig. 3B).

DISCUSSION

Distinguishing Primary Biosignatures from Secondary Alteration

The nature of sedimentary organics is determined by the molecular structure of their precursor biomass and by subsequent alteration

¹GSA Data Repository item 2019112, geological background, methods, description of the morphological and ultrastructural variations of organic matter in various stages of a cell cycle, Figure DR1, and Table DR1, is available online at <http://www.geosociety.org/datarepository/2019/>, or on request from editing@geosociety.org.

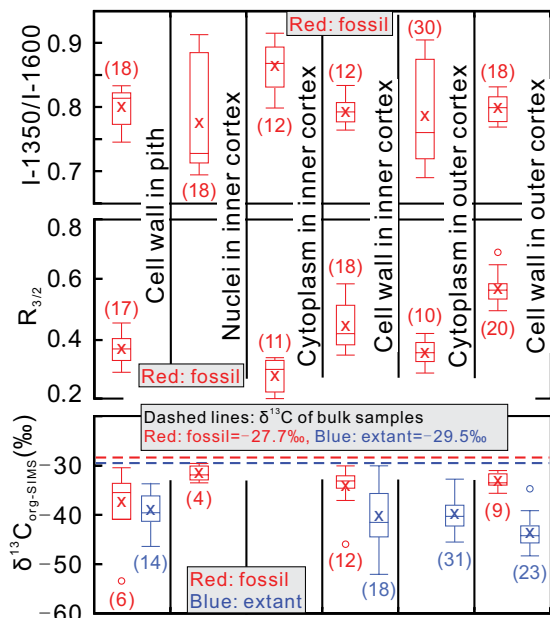


Figure 2. Summary box plots of Raman spectra parameter I-1350/I-1600 (intensity ratio of the 1350 cm^{-1} band versus the 1600 cm^{-1} band), Fourier-transform infrared spectroscopy (FTIR) carbon-chain branching index $R_{3/2}$ (intensity ratio of the 2955 cm^{-1} band versus 2925 cm^{-1} band), and $\delta^{13}\text{C}_{\text{org-SIMS}}$ (org—organic; SIMS—secondary-ion mass spectrometry; in per mil, Vienna Pee Dee belemnite) values obtained from fossil and extant ferns, with numbers of measurements collected in parentheses. In order to avoid artifacts, only $\delta^{13}\text{C}_{\text{org-SIMS}}$ values with a ^{12}C count of sample versus standard >0.07 are plotted here to interpret their geobiological meaning. Raw data and more details of SIMS are provided in Table DR1 and Figure DR1 (see footnote 1).

(Qu et al., 2015; Vajda et al., 2017, and references therein). The primary components of the plant cell wall are polysaccharides, including cellulose, hemicellulose, pectin, and in some cases lignin (Buchanan et al., 2015). These compounds contain few functional groups of CH_2 , as indicated by higher $R_{3/2}$ values (Figs. 2 and 3). The structural order of organic remains derived from polysaccharides in cell walls did not change markedly during the cell cycles as implied by the relatively constant I-1350/I-1600 of cell walls compared to that in the nucleus and cytoplasm (Figs. 1 and 2). In contrast, the cytoplasm and membrane contain abundant CH_2 on the long carbon chains (e.g., lipids and proteins), as indicated by lower $R_{3/2}$ values of the cytoplasm from both the inner and outer cortex compared to their cell walls (Figs. 2 and 3). This observation is consistent with a previous study on Devonian (410 Ma) fossilized plants from Rhynie chert (Scotland) (Qu et al., 2015). The nucleus and cytoplasm contain abundant heteroatoms (e.g., P, N, S, O, H, in the protein and

nucleic acid, and other metal elements such as Ca, Mg, K). Moreover, the molecular structures of nucleic acids (DNA and RNA) vary significantly during mitosis (Buchanan et al., 2015). Therefore, the diverse chemical compositions of the carbon precursors could explain the marked molecular structural variations in the organic remains of the fossilized nucleus and cytoplasm, as recorded by larger variations in I-1350/I-1600 relative to that of the cell walls (Figs. 1 and 2).

The carbon isotopic composition of an organism is determined by its assimilated carbon source and the metabolic pathways utilized (Hayes, 2001). The similarity in carbon isotopic values between the fossil ($\delta^{13}\text{C}_{\text{org-bulk}} \sim -27.7\text{‰}$) and extant (-29.5‰ ; Fig. 2) fern implies the same metabolic pathway and coincides with evolutionary stasis as proposed for the fossil Osmundaceae (Bomfleur et al., 2014). The minor difference (1.8‰) in $\delta^{13}\text{C}_{\text{org-bulk}}$ observed between the fossil and extant ferns (Fig. 2) could perhaps reflect slightly ^{13}C -enriched Jurassic atmospheric CO_2 globally and/or locally, or

different water-use efficiency (Farquhar and Richards, 1984) induced by dissimilar Jurassic atmospheric CO_2 concentration. Alternatively, the higher $\delta^{13}\text{C}_{\text{org-bulk}}$ (by 1.8‰) of the fossil may result from the preferential loss of isotopically light compounds combined with the preservation of ^{13}C -enriched organic remains during post-depositional processes (Clayton, 1991), which is consistent with the higher average $^{13}\text{C}_{\text{org-SIMS}}$ values from the fossil fern (Fig. 2).

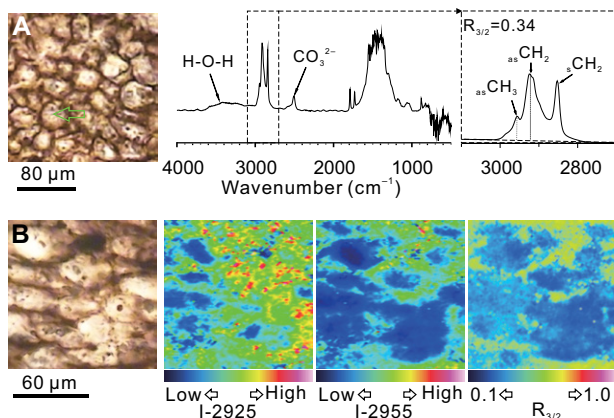
Concerning the *in situ* carbon isotope measurements, the low $^{13}\text{C}_{\text{org-SIMS}}$ values from the extant fern could be the result of a matrix effect related to the presence of water. House (2015) showed that hydrated organic materials cause a matrix effect during SIMS analysis, leading to an apparent observed ^{13}C depletion. Because we used graphite as a standard (virtually free of water) during the analysis of the hydrous extant fern sample, we likely caused this water-related matrix effect. In the fossil fern, this effect may have been less, because the material is less hydrous than in the extant fern. It is therefore important to note that we do not interpret the absolute $^{13}\text{C}_{\text{org-SIMS}}$ values, but only the internal variations within the extant and fossil ferns, respectively.

The variations of $^{13}\text{C}_{\text{org-SIMS}}$ in different cellular organelles (Fig. 2) possibly reflects diverse organic compounds with heterogeneous isotopic compositions. Indeed, isotopically heterogeneous cellular compounds from modern terrestrial plants with ^{13}C variations $>10\text{‰}$ have been reported (e.g., Collister et al., 1994). However, terrestrial plant compounds preserved in sediments generally have less carbon isotopic heterogeneity (variations in $\delta^{13}\text{C}$ of a few per mil; e.g., Naraoka and Ishiwatari, 2000). In this study, the narrower ranges of $^{13}\text{C}_{\text{org-SIMS}}$ (Fig. 2) from the fossil fern could imply preferential decomposition and preservation of certain compounds (Igisu et al., 2009) during post-depositional processes, and thus the taphonomic processes seem to have diminished the subcellular isotopic heterogeneities.

Ultrastructural Variations in Chromosomes during Mitosis

Here we characterize specifically the molecular structural variations of organic matter in the nuclei and chromosomes preserved in the cell cycle of the fossil Jurassic royal fern (see more details in Figs. 1E–1N; and in the Data Repository). The nucleus is a dynamic organelle whose morphology and chemical composition change across different stages of the cell cycle. The nuclear envelope and matrix, predominantly consisting of lipids, fibrin, protein, and minor RNA, decompose and reconstruct throughout mitosis (Buchanan et al., 2015). The nucleolus, consisting of abundant RNA and protein, is also highly dynamic and experiences transformation, decomposition, and regeneration in the cell cycle (Buchanan et al., 2015). The chromatin

Figure 3. Examples of micro Fourier-transform infrared spectroscopy spectra and maps obtained from a fossil fern. A: Spectrum obtained from location illustrated by arrow; enlarged parts are used to calculate branching index $R_{3/2}$ (intensity ratio of the 2955 cm^{-1} band versus 2925 cm^{-1} band) of carbon chains. As—asymmetric, s—symmetric. B: Maps of intensity of 2925 cm^{-1} (I-2925) and 2955 cm^{-1} (I-2955) and $R_{3/2}$, indicating strength of asymmetric vibrations of CH_2 , CH_3 , and $R_{3/2}$, respectively.



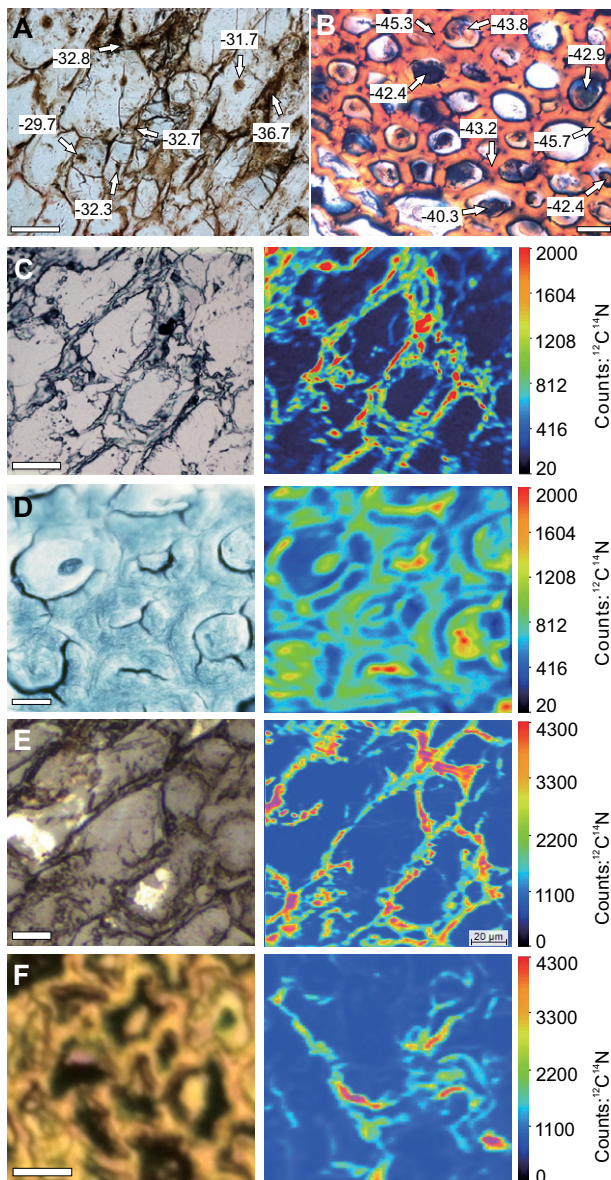


Figure 4. Examples of $\delta^{13}\text{C}_{\text{org-SIMS}}$ (org—organic; SIMS—secondary-ion mass spectrometry) values and SIMS maps. A,C,E: Fossil fern. B,D,F: Extant fern. A and B: Examples of actual positions (arrows) where SIMS analyses were performed, with obtained $\delta^{13}\text{C}_{\text{org-SIMS}}$ values. C–F: Optical microscopic images (reflected light) and corresponding SIMS maps of $^{12}\text{C}^{14}\text{N}$ counts, representing abundance of organic matter. Scale bars = 20 μm .

and chromosome have a chemical composition of mainly DNA and protein, with minor RNA. During mitosis, their chemical compositions and sequences of nucleotide generally remain unchanged, but molecular structures of the DNA chains experience three-dimensional packaging, folding, and twining with the involvement of various enzymes (Buchanan et al., 2015). This could be a reason for more-pronounced molecular structural variations in the nuclei, as is indicated by large ranges of I-1350/I-1600 compared to other cellular organelles (Figs. 1 and 2).

Jurassic Mitosis “Frozen” in Time

Fossilization via silicification (e.g., Remy et al., 1994; Javaux et al., 2010) and fossilization via phosphatization (e.g., Hagadorn et al., 2006; Huldtgren et al., 2011) are the most common mechanisms for preserving subcellular structures in the fossil record, whereas permineralization of plant remains by calcite is

very rare. Our study is notable because Korsaröd is the only locality known to preserve the ongoing mitosis processes in Jurassic plant cells via calcification from volcanic hydrothermal brine (Figs. 1E–1N). The permineralization process probably started when the plant was still alive and absorbed the carbonate-rich brine that subsequently filled individual cells as the brine infiltrated the rhizome (maps of I-Cal in Figs 1E–1N). The rapid calcite permineralization “froze” the organic molecules in time and chemically halted their decomposition, while also mechanically protecting the cytoarchitectures from breakdown during post-depositional processes. The absence of high-grade metamorphism enabled the exceptional preservation of the cellular organelles of the fossilized fern.

In summary, our research presents molecular structural and isotopic characteristics of organic remains in the cytoarchitectures of a fossil Jurassic fern, revealing the molecular

structural variations of nuclei and chromosomes during the cell cycle. The carbon isotopic similarity between fossil and extant ferns supports evolutionary stasis of this plant lineage since the Jurassic. The smaller subcellular isotopic variations of organic remains in the fossil compared to those of the extant fern possibly indicate a preferential decomposition and/or preservation of cellular compounds during taphonomic processes. Our study provides unprecedented insights into the characteristics and behaviors of cellular organelles of a Jurassic fern during the cell cycle and their preservation during post-depositional processes. This study also demonstrates the use of *in situ* techniques of Raman spectroscopy, micro-FTIR, and SIMS in studying ancient cellular organelles.

ACKNOWLEDGMENTS

This project is financially supported by the National Key R&D Program of China (2018YFC0309800), the Hundred Talent Program C of China (Y810011BRC), the Swedish Research Council (VR 2015-04264), the Bergen Research Foundation (Norway), the European Research Council under the European Union’s Horizon 2020 research and innovation program (grant agreement 646894), and the Department of Science and Technology–National Research Foundation Centre for Excellence in Palaeosciences at the University of Witwatersrand (South Africa). The NordSIM laboratory at the Swedish Museum of Natural History is a Vetenskapsrådet (VR)-funded research infrastructure, of which this is publication 593. We highly appreciate the technical assistance of the University of Bergen, the Institut de Physique du Globe de Paris, the MAX Lab at Lund University, and the NordSIM lab. Many thanks to Gang Lü for helping us with data processing, and to the Botanical Garden in Lund for providing extant royal fern samples.

REFERENCES CITED

- Bomfleur, B., McLoughlin, S., and Vajda, V., 2014, Fossilized nuclei and chromosomes reveal 180 million years of genomic stasis in royal ferns: *Science*, v. 343, p. 1376–1377, <https://doi.org/10.1126/science.1249884>.
- Buchanan, B.B., Grissem, W., and Jones, R.L., eds., 2015, *Biochemistry and Molecular Biology of Plants* (second edition): John Wiley & Sons, 1280 p.
- Clayton, C.J., 1991, Effect of maturity on carbon isotope ratios of oils and condensates: *Organic Geochemistry*, v. 17, p. 887–899, [https://doi.org/10.1016/0146-6380\(91\)90030-N](https://doi.org/10.1016/0146-6380(91)90030-N).
- Collister, J.W., Rieley, G., Stern, B., Eglinton, G., and Fry, B., 1994, Compound-specific $\delta^{13}\text{C}$ analyses of leaf lipids from plants with differing carbon dioxide metabolisms: *Organic Geochemistry*, v. 21, p. 619–627, [https://doi.org/10.1016/0146-6380\(94\)90008-6](https://doi.org/10.1016/0146-6380(94)90008-6).
- Farquhar, G.D., and Richards, R.A., 1984, Isotopic composition of plant carbon correlates with water-use efficiency of wheat genotypes: *Functional Plant Biology*, v. 11, p. 539–552, <https://doi.org/10.1071/PP9840539>.
- Hagadorn, J.W., et al., 2006, Cellular and subcellular structure of Neoproterozoic animal embryos: *Science*, v. 314, p. 291–294, <https://doi.org/10.1126/science.1133129>.
- Hayes, J.M., 2001, Fractionation of the isotopes of carbon and hydrogen in biosynthetic processes: *Reviews in Mineralogy and Geochemistry*, v. 43,

- p. 225–277, <https://doi.org/10.2138/gsrmg.43.1.225>.
- House, C.H., 2015, A synthetic standard for the analysis of carbon isotopes of carbon in silicates, and the observation of a significant water-associated matrix effect: *Geochemical Transactions*, v. 16, p. 14, <https://doi.org/10.1186/s12932-015-0029-x>.
- Huldtgren, T., Cunningham, J.A., Yin, C., Stampanoni, M., Marone, F., Donoghue, P.C.J., and Bengtson, S., 2011, Fossilized nuclei and germination structures identify Ediacaran “animal embryos” as encysting protists: *Science*, v. 334, p. 1696–1699, <https://doi.org/10.1126/science.1209537>.
- Igisu, M., Ueno, Y., Shimojima, M., Nakashima, S., Awramik, S.M., Ohta, H., and Maruyama, S., 2009, Micro-FTIR spectroscopic signatures of bacterial lipids in Proterozoic microfossils: *Precambrian Research*, v. 173, p. 19–26, <https://doi.org/10.1016/j.precamres.2009.03.006>.
- Javaux, E.J., Marshall, C.P., and Bekker, A., 2010, Organic-walled microfossils in 3.2-billion-year-old shallow-marine siliciclastic deposits: *Nature*, v. 463, p. 934–938, <https://doi.org/10.1038/nature08793>.
- Naraoka, H., and Ishiwatari, R., 2000, Molecular and isotopic abundances of long-chain *n*-fatty acids in open marine sediments of the western North Pacific: *Chemical Geology*, v. 165, p. 23–36, [https://doi.org/10.1016/S0009-2541\(99\)00159-X](https://doi.org/10.1016/S0009-2541(99)00159-X).
- Qu, Y., Engdahl, A., Zhu, S., Vajda, V., and McLoughlin, N., 2015, Ultrastructural heterogeneity of carbonaceous material in ancient cherts: Investigating biosignature origin and preservation: *Astrobiology*, v. 15, p. 825–842, <https://doi.org/10.1089/ast.2015.1298>.
- Qu, Y., Wang, J., Xiao, S., Whitehouse, M., Engdahl, A., Wang, G., and McLoughlin, N., 2017, Carbonaceous biosignatures of diverse chemotrophic microbial communities from chert nodules of the Ediacaran Doushantuo Formation: *Precambrian Research*, v. 290, p. 184–196, <https://doi.org/10.1016/j.precamres.2017.01.003>.
- Qu, Y., Zhu, S., Whitehouse, M., Engdahl, A., and McLoughlin, N., 2018, Carbonaceous biosignatures of the earliest putative macroscopic multicellular eukaryotes from 1630 Ma Tuan-shanzi Formation, north China: *Precambrian Research*, v. 304, p. 99–109, <https://doi.org/10.1016/j.precamres.2017.11.004>.
- Remy, W., Taylor, T.N., Hass, H., and Kerp, H., 1994, Four hundred-million-year-old vesicular arbuscular mycorrhizae: *Proceedings of the National Academy of Sciences of the United States of America*, v. 91, p. 11,841–11,843, <https://doi.org/10.1073/pnas.91.25.11841>.
- Schiffbauer, J.D., Xiao, S., Sharma, K.S., and Wang, G., 2012, The origin of intracellular structures in Ediacaran metazoan embryos: *Geology*, v. 40, p. 223–226, <https://doi.org/10.1130/G32546.1>.
- Vajda, V., Pucetaite, M., McLoughlin, S., Engdahl, A., Heimdal, J., and Uvdal, P., 2017, Molecular signatures of fossil leaves provide unexpected new evidence for extinct plant relationships: *Nature Ecology and Evolution*, v. 1, p. 1093–1099, <https://doi.org/10.1038/s41559-017-0224-5>.

Printed in USA